ICAS-88-4.5.1

EFFECTIVENESS OF COMBINATION OF APEX AND LEADING-EDGE VORTEX FLAP ON A 74 DEGREE DELTA-WING WITH OR WITHOUT TRAILING-EDGE FLAP

T.D.Hsing*,K.X.Shen**,Z.F.Wang†,W.H.Guo***,F.G.Zhuang*

Beijing University of Aeronautics and Astronautics,Beijing,P.R.China

Abstract

Experimental methods including the aerodynamic pressure and force measurements, the seven-hole probe to survey the velocity distribution in the cross flow plane as well as the new technique using the hydrogen bubble and LASER sheet for flow visualization were conducted to study the effect of apex flap and trailing-edge flap on the aerodynamic characteristics of a 74 degree swept delta wing equipped with leading-edge vortex flap.

As usual, the leading-edge flap acts well in reducing the drag, but diminishing the lift at lower angle of attack. However, the nose-up deflected apex flap along with the tail-down deflected trailing-edge flap can increase the lift prominently, accompanying with a slight decrease of lift-drag ratio at higher angle attack and more at lower angle of attack. To deflect only the apex flap nose-up will raise the lift-drag ratio for entire region of angle of attack tested, while a mild reduction of lift appears. As we found, fitting the apex flap and the trailing-edge flap on a highly swept delta-wing equipped with leading-edge vortex flap will have advantages in increasing the lift and the lift-drag ratio.

A discrete vortex method based on the slender body theory has been applied to compute the roll-up of vortices shedding from the leading-edge, and the pressure distribution on the flap and wing. The numerical results simulate well the roll-up of vortex-layer as examplified by a comparison of the figures with that observed in the flow visualization. The surface pressure distribution in the same cross flow plane have a similar pattern both for the computational and experimental results.

1. Introduction

The modern advanced supersonic fighters appear to have thin, highly swept, slender wings for the sake of reducing the wave drag. However, on these wings the flow separates from the leading edge at moderate angle of attack in subsonic and transonic range. The separated flow rolls up into vortices causing a drag increase and a decrease in lift-drag ratio owing to the loss of leading edge suction.

In order to minimize the excessive drag rise at higher angle of attack, the concept of employing vortex flap was suggested in late seventies(1)(2). That is, by tilting the leading-edge vortex flap downwards, the pressure force acting on the flap will produce a thrustwise component effective in reducing the drag and raising the lift-drag ratio accompanying with a deficiency of slight lift reduction. For the slender wing, actually there are drawbacks such as too large drag at large angle of attack and too small lift at small angle of attack. The use of vortex flap at the leading edge can reduce the drag with reduction of lift. In order to get an improvement in the performance of take-off, landing and manoeuvrability, another measure must be sought. As to increasing the lift, the strake which has been utilized extensively on wings of high speed fighters seems inadequate here for the highly swept slender wing, because of its degradation of lift production. In late years, the use of apex flap to produce more lift has been proposed(3). The apex flap so called is a foremost part of the delta wing which can be deflected up and down around a spanwise axis. The addition of apex and trailing edge flaps on the delta wing has been proved effective in increasing lift(3) at the cost of drag penalty. On the other hand, as explained above, the leading edge vortex flap has the ability of reducing the drag but producing less lift. As it is ,the disadvantages of leading edge vortex flap happen to be the advantages of a combination of apex flap and trailing edge flap, it seems that to attach both the apex and leading edge flaps on a slender wing equipped with trailing edge flap, which they are complementary to one another, will yield abetter results as we expected. For the purpose of verifying the effectiveness of the combination, we chose 74 degree swept delta planform as a basic wing furnished with detachable constant chord leading edge vortex flap which is named model A and two types apex flap to be fitted on as sketched in Fig.1. The latter two models are named model B and model C respectively. The results of low speed experiments and computation have primarily born out the validity of our concept in improving the aerodynamic characteristics of highly swept wing.

2. Notations

x,y,z	wing-fixed coordinates with origin at wing apex according to Fig.2
s	local delta wing half span
c	center-line chord of the wing
S	wing area
A	wing aspect ratio ($A=4s^2/S$)
U_∞	free stream velocity
p_o	total pressure
p	static pressure
q_∞	free stream dynamic pressure ($q=\rho U_\infty^2/2$)
c_{po}	total pressure coefficient ($c_{po}=\frac{p_o-p_\infty}{q_\infty}$)
c_p	static pressure coefficient ($c_p=\frac{p-p_\infty}{q_\infty}$)
c_L	lift coefficient ($c_L=L/Sq_\infty$)
c_D	drag coefficient ($c_D=D/Sq_\infty$)
K	lift-drag ratio ($K=c_L/c_D$)
p_∞	free stream static pressure

This work was supported by the research fund of contract no.86A51002 under administration of Ministry Aviation Industry, P.R.China

*Professor, **Associate professor, ***Graduate student, †Lecturer.

c_m	pitching moment coefficient ($c_m=M/Sq_\infty c$)
ϕ	velocity potential of perturbation
u	local velocity
u_i	velocity of the vorticity shedding from the leading edge
u_x, u_y, u_z	component of local velocity in the wing-fixed coordinates
α	angle of attack
γ	strength of vortex segment
δ_V	deflection angle of leading-edge vortex flap
δ_F	deflection angle of apex flap
δ_H	deflection angle of trailing-edge flap
ξ, η, ζ	nondimensional coordinates,

3. Models and experimental set-up

3.1 Models

The model of basic delta wing used for balance measurements is made of 4mm thick duralumin plate and has a semi-span length of 165mm and total area of 949.5cm^2. The leading-edge vortex flaps and trailing-edge flaps were cut from 0.8mm thick duralumin plate and hinged to the basic wing. The edges are all sharpened to enhance flow separation. The apex flap of model B was obtained by cutting the foremost part of the basic delta and incorporating a transverse hinge at x/c=16.6% with its leading edge staggered in from the leading-edge of vortex flaps. The leading edge of the apex flap of model C is in alignment with the leading edge of vortex flap thus keeping the whole planform a delta form, and its hinge line located at x/c=26.9% from the apex. Details of the models are given in Fig.1.

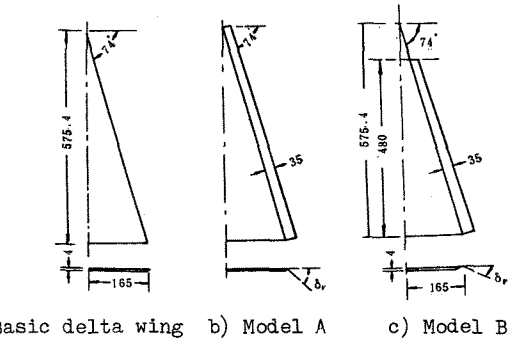

a) Basic delta wing b) Model A c) Model B

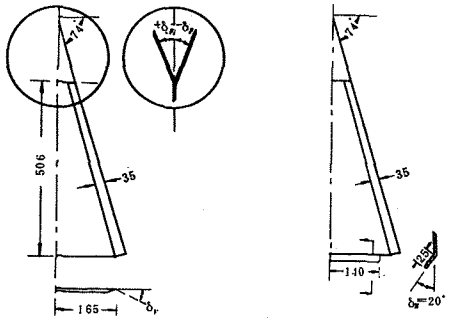

d) Model C e) Model C with trailing-edge flap

Fig.1. Wing model planforms

3.2 Testing facilities

Experiments were carried out in turn, in low speed wind tunnels and water channel at BUAA, Beijing, and wind tunnel of Aerodynamic Development Center of China in Sichuan Province, China. The facilities are as follows:

D-4 windtunnel Having a test section of closed circular type with a diameter of 1.5m and a useful length of 2m. The models were mounted on the strut of a six-components mechanical balance having a variable pitch angle system with a range of approximately -4° to 30°. The maximum wind speed is 35 m/sec.

ADCC windtunnel A closed test section is 1.4m high and 1.4m wide with a useful length of 3m. The models were mounted on a strain gage balance sting which can be rotated to vary the pitch angle from -4° to 30°. The wind speed was kept at 30m/sec for testing.

D-1 windtunnel A closed circuit wind tunnel with an elliptical test section having a span of 1.02m and jet height of 0.75m. The maximum speed is 35m/sec.

BUAA water channel It is of horizontal type having a 40cm×40cm test section. The flow speed ranges from 10cm/sec to 20cm/sec.

3.3 Description of the tests

Flow field visualization New techniques by using hydrogen bubble and LASER sheet were conduted to visualize the vortex patterns. A fine platinum wire is placed in front of the leading edge to serve as the cathode of a D.C. current. The bubbles were illuminated by a 0.5mm-1.0mm thick narrow LASER sheet directed normally to the x-axis (Fig.2) within the BUAA water channel.

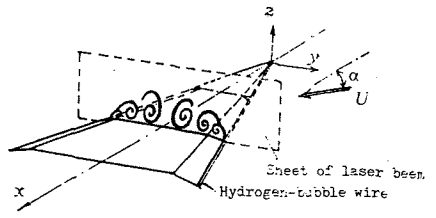

Fig.2. Sketch of the test-device

Flow field measurements They were conducted by using a conical seven-hole probe with a diameter of 2.5mm (Fig.3) to measure the distribution of total pressure, static pressure as well as the flow direction in the cross flow plane. The probe is available for measuring highly deviated flow up to an angle of attack about 60°. Tests were carried out

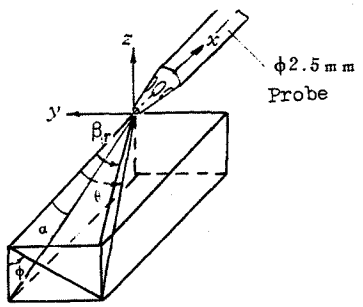

Fig.3. Conical seven-hole probe and the coordinates of measurement

in D-1 wind tunnel with Re=0.9X10^6. The flow field around model C at α=15° and δ_F=-10°,0°,10° were successively measured in planes of x/c=0.5,1.0,1.09.

Pressure measurements The measurements were carried out in the ADCC wind tunnel. A specially designed half-model wing was fabricated for measuring the pressure distribution on the upper surface of the wing. The static pressure orifices equipped were perpendicular to the free stream, each orifice was connected to a scanning valve with transducer to record and transmit the pressure signal to a computer for data processing.

Balance measurements A strut-type mechanical balance was adopted together with a computer used for data recording and processing. For all models three-component measurements were carried out in the $-4^\circ \leq \alpha \leq 30^\circ$ angle of attack range in the D-4 wind tunnel with Re=1.1X10^6.

4. Discussion of results

4.1 Constant chord vortex flaps

The pattern of the flow passing around the model equipped with constant chord vortex flaps can be seen clearly from the water tunnel. For example we can see the manner of the flow separation from the leading edge and the roll-up of the vortex layer for α=15° at x/c=0.5 in Fig.4. There are also total pressure contours and velocity distribution graphs where two minimum total pressure points corresponding to the main and the secondary vortex centers can be found. It is obvious, if the vortex attachment can be prevented from moving onto the main delta wing, the negative peak pressure will remain over the vortex flap, producing strong drag reduction effect. Actually, it is difficult to maintain such an ideal flow pattern along the x-axis, as the flow moves from apex towards the trailing edge. In the past, a lot of measures have been plotted by means of modifying the shape of the vortex flap in an attempt to strengthen the drag reduction effect(5). On the other hand, one can achieve this object by utilizing the advantage of vortex interaction such as we intend to study by using apex flap.

The balance measurements have born out that on the whole the vortex flap functions better at δ_v=30° than flaps at other δ_v tested. Therefore for all tests reported here, we kept δ_v=30°. The curves indicating the aerodynamic characteristics of model A including c_L-α, c_L-c_D, K-c_L and c_m-c_L relations are given in Fig.5. Comparing these curves with that of the basic delta wing, it is obvious that the drag decreases and the lift-drag ratio increases appreciably with a weak reduction of lift. In addition, the pitching moment curve is nearly linear and the stalling angle is postponed due to the delay of vortex breakdown.

4.2 Aerodynamic effects of the apex flap

We have two kinds of apex flap equipped on the model B and model C, the latter has been studied in more detail. For the model C, the flow visualization experiments were taken in turn for α=7°,15° and the deflection of apex δ_F=-10°,0°,10° in the water channel. Photographs are given in Fig.6 showing how the vortex originating from the apex flap are growing as it moves into the region above the basic delta wing and the vortex shedding from the leading edge of vortex flap. From the c_L-α curve it can be recognized that α=7° and 15° are nearly corresponding to the state of c_L/c_D maximum and c_L=0.5 respectively.

Flow pattern From the pictures in the Fig.6 a) and b), we can see that at α=7°, the flow is basically attached to the upper surface of the apex flap no matter how large the deflection δ_F may be, although the flow pattern is different for different δ_F. When the apex flap is tilted nose-down to δ_F=-10°, no vortex originating from the edge of apex flap can be discerned, because the apex flap has a locally negative α. Rotating the deflection of apex flap upwards to δ_F=0, now the flap having a positive local α will render the flow to develop into vortex after separating from the leading edge. This developed vortex extending down-stream till close to the trailing edge can be discerned in the pictures for all α tested. Increasing δ_F to δ_F=10°, we can obviously see the scale of the vortex is enlarged because of the large local angle of attack now reached. In the Fig.6 c) and d), photographs shown are the flow patterns visualized at α=15°. Comparing these pictures with that of α=7°, we can find the strong vortices separated from the leading edge flap and apex flap for all δ_F tested gradually merge to each other as they move downstream. For α=10° case, the vortex of apex flap seems to spread out and the velocity induced in the cross flow plane is so weak that it is not easily to be discerned, however we still can find their vague traces there. Maybe the breakdown has happened, causing the drag to increase and the lift-drag ratio to decrease as were confirmed by the experimental results of balance measurements to be explained later.

Component of velocity vector in the cross flow plane A seven-hole probe has been used after the method developed by K.N.Everett and A.A. Gerner(4) to measure the component of velocity in the cross flow planes. In Fig.7, the distributions of velocity component measured in planes at x/c=0.5 are presented. They are corresponding to apex flap de-

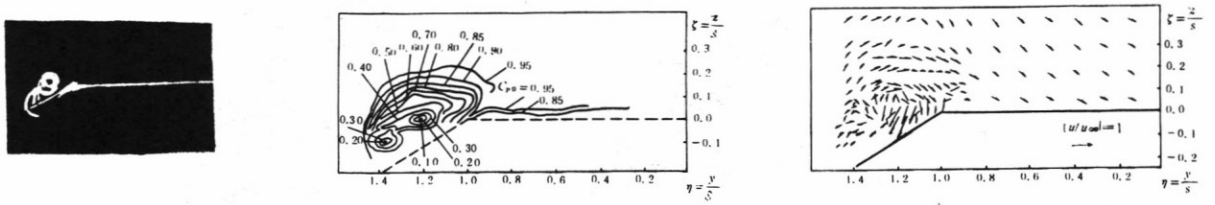

a) Flow visualization showing the vortex shedding

b) Contours of total pressure coefficient

c) Component of the velocity vector in the crossflow plane

Fig.4. Vortex formation of model A wing in the plane x/c=0.5 at α=10°

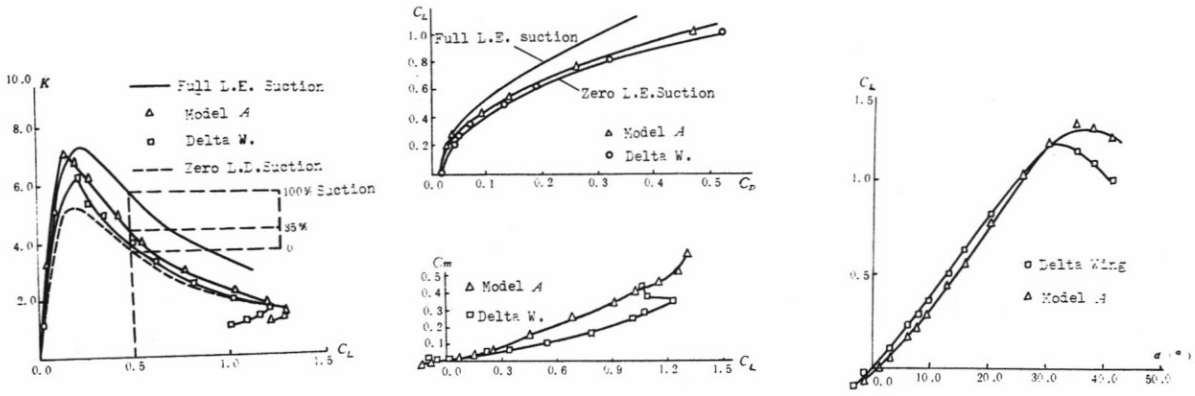

Fig.5 Aerodynamic characteristics of delta wing and model A

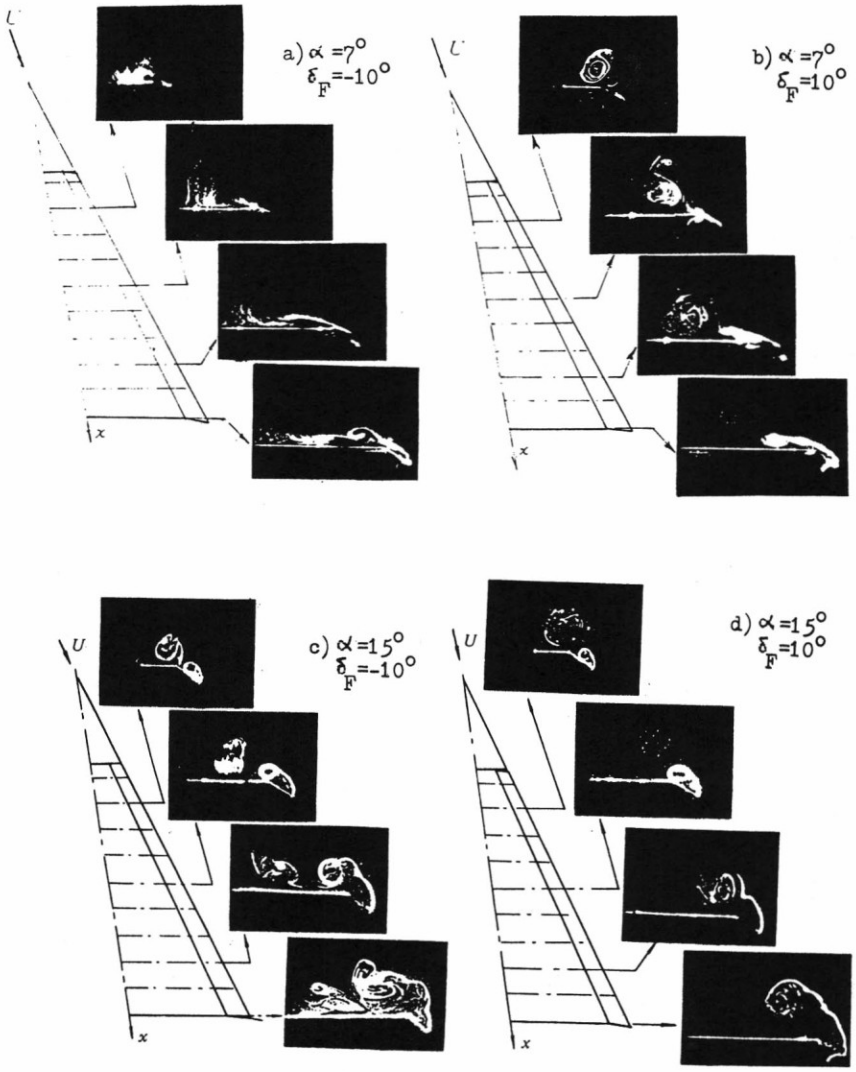

Fig.6 Flow field visualization showing vortices shedding from the leading edge of model C at δ_v=30°

flection δ_F=-10°,0°,10° at α=15°. In each of these graphs, two centers of vortex can be found clearly. The inner located over the main wing originated from the apex flap and the outer one at the position over the leading edge vortex flap is separated from the leading edge. After comparing these graphs, we can learn that to each center the nondimensional normal distance between the center and the wing surface, i.e. z/s, and the strength (the induced velocity components) of the vortex increases with the increase of angle δ_F, while its spanwise distance remains nearly unchanged. Here, for the inner center, the value of z/s increases from 0.28 through 0.37 to 0.46 as δ_F increases from -10° through 0° to 10° respectively, while y/s=0.46~0.53. Similarly, the outer one situated over the flap remains nearly at y/s=1.15~1.20 while its normal distance changes from 0.1 through 0.12 to 0.13.

The graphs shown in Fig.8 are the results measured in cross flow plane at x/c≒1.09, i.e. the plane at 9% of root chord behind the trailing edge. We still can find these two centers of vortex and their further movements away from the wing plane. The inner one raise from z/c≒0.03 through 0.1 to 0.14 as the apex flap deflection changes from -10° through 0° to 10° respectively, while y/s≒0.4. Similarly, the outer center of vortex separated from the leading edge remains spanwise nearly at y/s≒0.97 as its normal distance z/c changes from 0.08 through 0.13 to 0.16, while the δ_F increases from -10° through 0° to 10° respectively. Comparing the graphs of plane x/c=0.5 and x/c=1.09, we can find the scale of the vortex increases while the strength (the induced velocity component) decreases, and maybe in some cases like α=15°, δ_F=10°, the vortex has already broken down as we have explained according to the flow visualization pictures. As a whole, the outer vortex remains basically in the region above leading edge vortex flap because of the existence of inner vortex which effectively produces a beneficial interaction in retarding the inward wandering of outer vortex. The same phenomena can be observed in the flow visualization and the experimental results of pressure measurements.

Results of pressure measurements The pressure distributions on the wing surface at x/c=0.5 plane for α=10°,15°,20° and 30°, and at plane x/c=0.9 for α=10° and 25° are shown in Fig.9 and Fig.10. From the above figures, we discover that as a whole, the peak of suction appearing on the surface of leading edge vortex flap is the highest for δ_F=-10°, it decreases gradually as δ_F increases through 0° to 10° where the suction peak reduces to a minimum. These results reflect the flow patterns we have seen in the flow visualization tests and agree with the results of flow field measurements. As we have explained above, although the outer vortex center nearly comes to a standstill spanwisely, it will reach its higher normal position with respect to the wing surface, this will decrease the induced velocity near the wing surfsce and in turn the pressure as the deflection of the apex flap increases in the positive direction. As the pressure curve for plane x/c=0.5 shown in Fig.9, the spanwise distance y/s remains nearly unchanged at 1.15 that agrees with the value obtained from velocity mearsurement in cross flow plane. As to the inner vortex, the situation is quite opposite. Here, the suction is high at δ_F=10°, less at 0° and became the least at -10°, maybe it is due to the strength of the inner vortex turns stronger as δ_F increases, although the normal distance raises accompanying with. As a whole, the more lifting force contributed by th basic delta

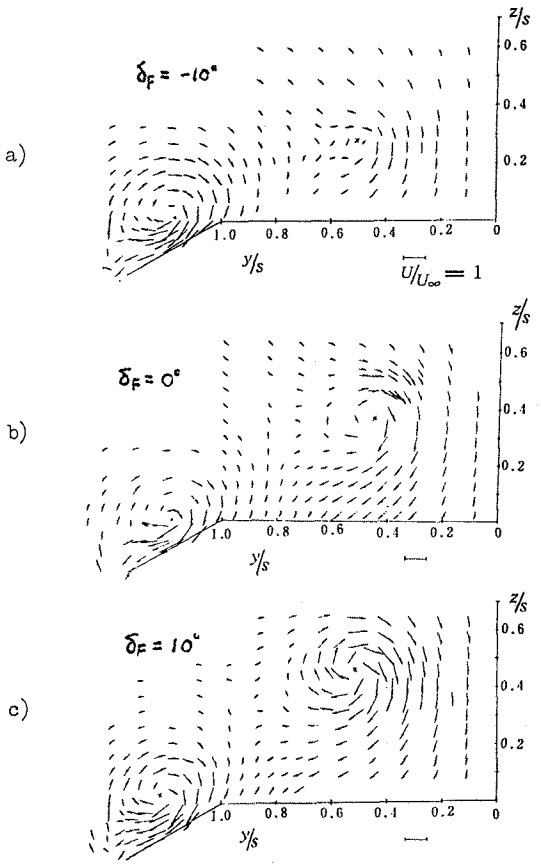

Fig.7 Velocity component vector in the plane x/c=0.5 at α=15°

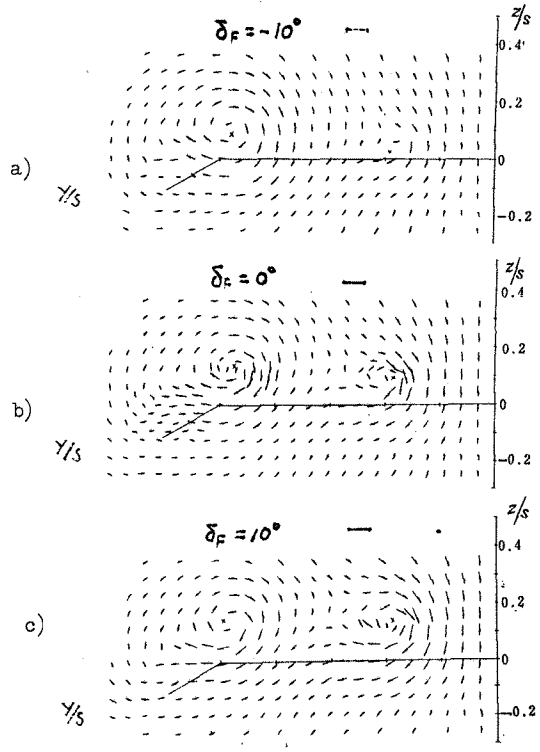

Fig.8 Velocity component vector in the plane x/c=1.09, behind the trailing edge, at α=15°

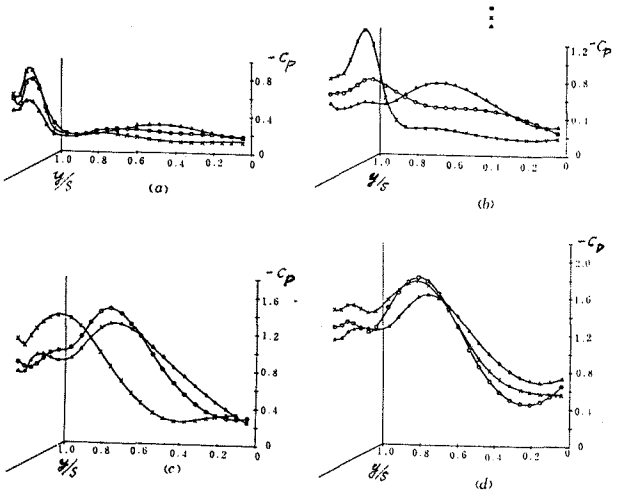

Fig.9 Pressure distribution curves for plane x/c=0.5 a) α=10° b) α=15° c) α=20° d) α=30°, ×-- δ_F=-10°, ○-- δ_F=0°, △-- δ_F=10°

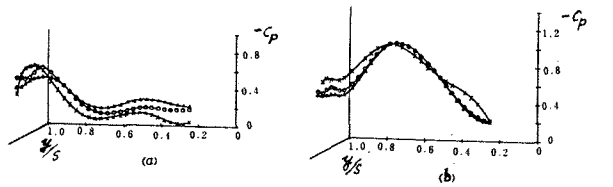

Fig.10 Pressure distribution curves for x/c=0.9 plane a) α=10° b) α=25°

wing for positive δ_F may be compensated by the lifting capacity lost at the leading edge vortex flap, and vice versa when δ_F becomes negative. This may be the reason that the lift is nearly unchanged no matter the δ_F deflects in either direction as will be seen from the results of balance measurements later. Looking over the pressure distribution curves in Fig.9 for the plane x/c=0.5 as example, it appears that the position of suction peak on the vortex flap moves inwards to the main wing as α increases from 10° to 30°. On the other hand, the suction peak induced by the inner vortex moves in opposite direction from inner towards outside. Gradually, the two peaks draw in closer and closer and finally merge together at α=25°~30°. In the mean time, these three pressure distribution curves corresponding to δ_F=-10°,0°, 10° tend to coincide as α increases over 25°.

Comparing again the pressure distribution over vortex flap at plane x/c=0.5, the suction peaks appear on all three pressure curves corresponding to δ_F=-10°,0°,10° at lower angle of attack as α=10°. When α increases, the pressure idstribution curve of δ_F=10° becomes flater and the peak disappears. Then when α=20°, the flatness of δ_F=0° curve appears too. As α reaches to 25°, pressure peaks could hardly be found in all three pressure curves. That means the outer vortex has gradually become unstable and the vortex breakdown phenomena may be realized.

The pressure distribution curves of plane x/c=0.9 for α=10° and 25° are given in Fig.10, where we can still find the suction peak on the flap region is higher at δ_F=-10° than the other two curves and the situation is opposite for the suction peak on the main wing region, similar to that appearing in plane x/c=0.5. These three curves are much closer to one another with lower value of c_p in this cross flow plane as the trailing edge approached.

4.3 Computation of discrete vortex method based on slender body theory

The roll-up of vortices shedding from the leading edge and the pressure distribution on the flap and wing have been calculated for plane x/c=0.5 at α=15° as shown in Fig.11,12, based on the method of distributing discrete vortices in the cross flow planes has been developed on the basis of slender body theory. the fundamentals of this method is described in the appendix.

From Fig.11 we can see the computational shapes of the separated vortices and their similarity to that got from visualization as indicated in Fig.6 where the inner and outer vortices can be seen clearly. A family of pressure coefficient increment (Δc_p) curves for different δ_F ranging from -6° to 6° has been calculated and drawn in Fig.12, where the change of inner and outer suction peak as δ_F varies from -10° to 10° presents the same tendency, that is the outer Δc_p peak becomes larger than that of inner peak for $\delta_F \geq 0$ and vice verse for $\delta_F < 0$, as we have discussed before about the results of pressure measurements. The Δc_{pv} comprises the contribution presented by the vorticity γ in x direction of the cross flow plane considered, which corresponds to major term $(-\frac{u_x}{U_\infty})^2$ in c_p expression, accounting mainly the contribution of two separated vortices over the half-span to the pressure.

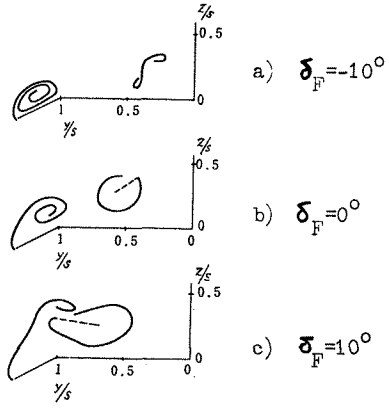

Fig.11 Roll-up separated vortices over model C computed for cross flow plane x=0.5 at α=15°

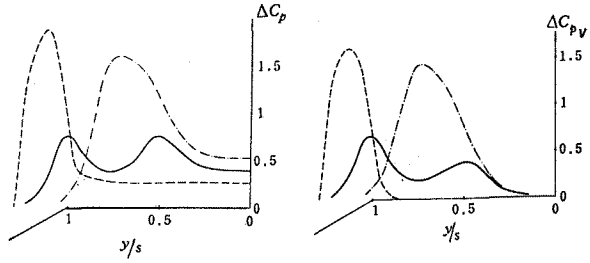

a) Pressure cofficient increment, Δc_p b) Main part of c_p contributed by $(\frac{u_x}{U_\infty})^2$, Δc_{pv}

Fig.12 Pressure coefficient increment of model C computed for cross flow plane x=0.5 at α=15° with δ_F=-10°,0°,10°

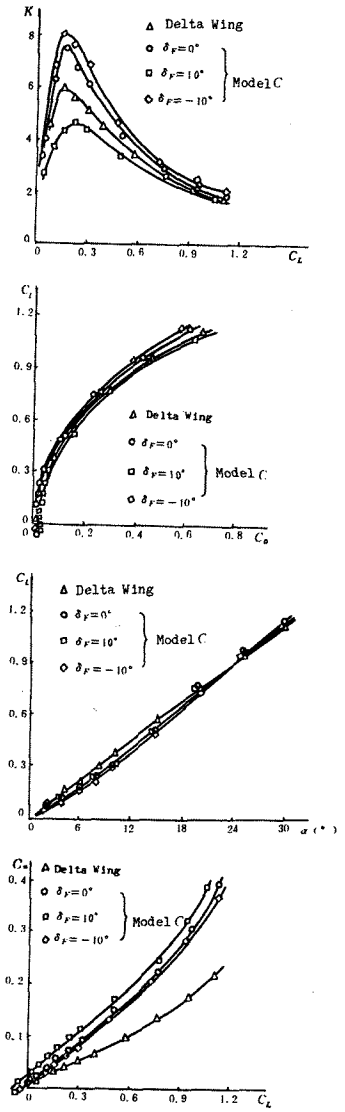

Fig.13 Aerodynamic characteristics of model C

4.4 Results of balance measurements

Model A For the case of model A, i.e. the basic delta wing having leading edge vortex flap with $\delta_V=30^\circ$, the aerodynamic characteristics such as $c_L\sim\alpha$, $c_L\sim c_D$, $K\sim c_L$ and $c_m\sim c_L$ curves obtained from the balance measurements are represented in Fig.5 accompanying with curves of the basic delta wing and the $K\sim c_L$, $c_L\sim c_D$ curves corresponding to zero or full suction for convenience of comparision. It should be noted that the aerodynamic coefficients of the basic delta wing with or without the leading edge vortex flap (according to the Polhamus analogy) were calculated referring to the projected area of their own plane form, i.e. the reference areas are different in each case. However, the moment reference center is at the centroid of basic delta and is the same for all plane forms.

From the $c_L\sim\alpha$ curves, it can be noticed that the vortex flap has two effects: One is the effect of a weak decrease of lift at $\alpha=0^\circ\sim26^\circ$ range, because of smaller local angle of attack at flap due to the deflection of δ_V and the forward inclination of the lift vector there, the other is to increase the c_{Lmax} and the corresponding critical angle of attack because of capability to delay the vortex breakdown just like we have seen in the flow visualization that the breakdown point has already reached the trailing edge at $\alpha=26^\circ$.

From the $K\sim c_L$ curves, we can see that the lift-drag ratio K has been improved quite a lot after attaching the vortex flap on the basic delta wing with $\delta_V=30^\circ$ due to the powerful effect of vortex flap in decreasing the drag, although the c_L slightly decreases. For example, we have 13% increase of K_{max} as well as 20~25% decrease of induced drag and about 20% increase of K at $c_L\doteq0.4$ 0.6 range.

As to the drag coeffient, the c_D value is nearly equal to that with full suction at $\alpha<10^\circ$ as the separated vortex being situated comletely above the flap. After that, the vortex will move inward to the region over main delta wing and thus it renders the drag reduction to diminish gradually, yet it will keep the c_D always smaller than that without the suction force.

The $c_m\sim c_L$ curve of model A becomes more linear due to the existence of vortex flap and the delay of vortex breakdown.

Model C and its combination with trailing edge flap Model C, one of the model with apex flap (Fig.1), has been taken as a main case in studying the effect of apex flap to improve the aerodynamic characteristics. We still set the deflection of the leading edge flap $\delta_V=30^\circ$ and three deflections of apex flap, i.e. $\delta_F=-10^\circ,0^\circ,10^\circ$ to carry out the balance measurements. The results gained are shown in Fig.13 with corresponding curves for the basic wing. In comparison with the basic wing, it reveals that the model C still possesses the property of lower lift at moderate and low α range (we have mentioned similar property of leading edge vortex flap). One important result is the deflection of apex flap gives no apparent influence on lift whether δ_F is positive or negative. This result is also true for model B according to the exeriments and agrees with that data in references (3). However, judging from the $c_m\sim c_L$ curves which are different for different deflection of apex flap, we can find that the pitching up moment is lager for model C with apex flap nose-up than that with nose-down. This means the lift exerting on apex flap has to be larger for apex flap nose up than for nose down. This deduction together with the inference that the total lift is nearly independent on the deflection of δ_F makes us now to have the conclusion that the lift contributed by afterpart of wing behind the apex flap should be larger for $\delta_F<0$ case than that of $\delta_F>0$. Looking over the graphs shown in Fig.9 to Fig.12, where the curves of pressure measurement and computation have been given, the loading on wing section is always larger for $\delta F<0$ than $\delta_F>0$, and this further substantiates the above conclusion.

If we attach the trailing edge flap on model C like the form shown in Fig.1 d), the combination will produce considerable increment of lift with flap deflected downward (the aerodynamic characteristic curves are given in Fig.14). At the same

time the drag will increase which renders the K_{max} decrease, but the persentage of decrease becomes smaller as the angle of attack increases, and in any case the K value will exceed that of model A.

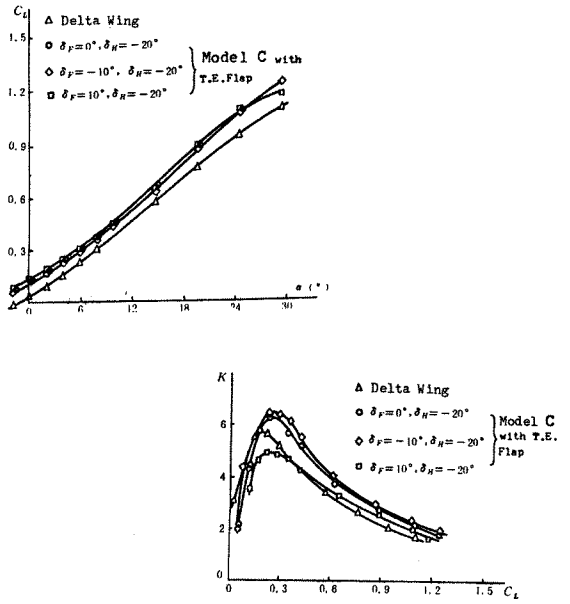

Fig.14 Aerodynamic characteristics of model C with trailing-edge flap

On the whole, deflecting the apex flap, K_{max} increase from about 7 in our experiments for the case of model A (delta wing plus leading edge flap) to 7.5 or 8 for model C (complete configuration with trailing edge flap detached), i.e. we have 7~14% increment of K, while the lift coefficient is only slightly reduced. As to the combination of apex flap, leading edge vortex flap and trailing edge flap on a 74 degree swept delta wing, it is found that downward deflection of trailing edge flap will cause the lift coefficient to increase while K_{max} decreases. However for larger angle of attack (8 degree for example) K become larger than that of model A.

The experimental results of model B show they are similar to that of model C. The aerodynamic characteristic curves of model C are given in Fig.15, to which no further discussion will be made.

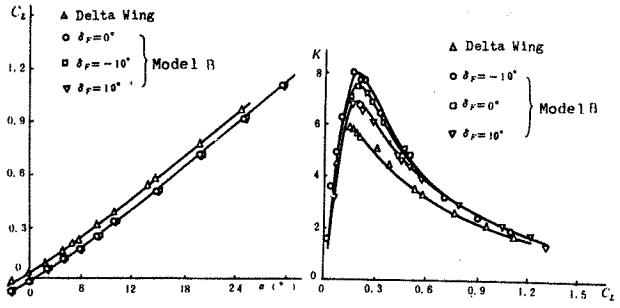

Fig.15 Aerodynamic characteristics of model B

5. Conclusion

Deflection of apex flap on a wing with leading edge vortex flap will not cause appreciable change in lift coefficient, however the pressure distributions are altered.

As the apex flap deflects downward ($\delta_F<0$), the pressure distribution on the leading edge vortex flap will yield a higher and higher suction peak, producing a large thrust component, so we have a better drag reduction effect and also with an increase in K. As the apex flap deflects upward (δ_F is from negative to positive), the pressure peak lowers with a decrease in K. This effect of leading edge vortex flap may be clearly seen from the force and pressure measurements, flow visualization tests. The computation based on our modified slender body theory also verifies the above statement.

A combination use of apex and trailing edge flap on a slender delta wing equipped with leading edge vortex flap will have the following effects: In the case of apex and trailing edge flaps are both deflected downward, lift will be appreciably increased and this will compensate the well-known defect of slender wing i.e., it has a smaller lift coefficient. But in so doing, the drag increases and the values of K at smaller angles of attack decrease; we also notice that with further increase in angle of attack, the decrease in K become less evident.

Based on what stated above, with a proper arrangement of the deflections of apex and trailing edge flaps we may arrive at desired lift increase, drag reduction and increase in lift-drag ratio in different flight regimes. This demonstrates the superiority of attaching apex and trailing flaps to a slender delta wing equipped with leading edge flaps.

6. References

(1) D.M.Rao: Leading Edge Vortex Flaps Experiment on a 74 Degree Delta Wing. NASA CR-159161, 1979.

(2) J.F.Marchman: Effectiveness of Leading Edge Vortex Flaps on 60 Degree and 74 Degree Delta Wings. J.of Aircraft,Vol.18,No.6, 1981.

(3) T.A.Buter & D.M.Rao: Force and Moment Measurements on a 74 Degree Delta Wing with Apex Flap. NASA CR-166081, 1984

(4) K.N.Everett, A.A.Gerner & D.A.Durston: Seven-Hole Cone Probes for High Angle Flow Measurement: Theory and Calibration. J.of AIAA, Vol.21,No.7, 1983.

(5) F.G.Zhuang, T.D.Hsing, Z.F.Wang, Z.J.Zhang & W.H.Guo: Aerodynamic Character of Vortex Flap and its Combination with Apex Flap. (Chinese) J.of BUAA, Vol.4, 1987. also ACTA Aerodynamica Sinica,Vol.6,No.1,1988.

(6) Z.Y.Lu, K.F.Xue & T.D.Hsing: Calculation of the Roll-up of Vortices Separated from the Leading Edge of Slender Wing. ACTA Aeronautica et Astronautica Sinica, Vol.9, No.9, 1988.

Appendix: Fundamentals of the discrete vortex method based on slender body theory

The method consists of the use of distribution of slices of vortex (or point vortex) to replace the wing and separated vortices based on the slender body theory in order to simulate the roll-up of vortices separated from the leading and trailing edges of slender wings and to calculate the load distribution on the surface (5). The method has the advantage of avoiding the difficulties encountered by using comformal transformation in the calculation for complex configurations as the conventional method usually made.

Based on the slender body theory for ideal incompressible flow, the potential perturbation function $\phi=\phi(y,z;x)$ should satify the Laplace equation in cross flow planes normal to the x-axis:

$$\frac{\partial^2\phi}{\partial y^2}+\frac{\partial^2\phi}{\partial z^2}=0 \qquad (1)$$

and the boundary conditions,

at far field: $\frac{\partial\phi}{\partial y}=0 \quad \frac{\partial\phi}{\partial z}=0$ (2)

on wing surface: $\frac{Df}{Dt}=0$ (3)

where $f(y,z;x)=0$ and $x=U\cdot\cos\alpha\cdot t$

on vortex sheet: zero force condition equivalent to the condition of coincidence of stream and vortex lines.

at leading edge: Kutta condition, zero normal velocity, $V_n\big|_{L.E.}=0$ (4)

In each cross flow plane, the wing section are divided into small segments. On each wing segment we have linearly distributed vorticity to replace the boundary and keep the vorticity strength on every neighboring segment equal at the section point. The boundary condition is to be satisfied at middle point of each wing segment. For every time step Δt, a new vortex piece of small stretch Δs will be born from the leading edge in line with the wing surface with $\Delta s=v_j\cdot\Delta t$, where v_j is the mean shedding velocity with which the new born vortex leaves from the leading edge. This new vortex piece willbe concentrated into a point vortex which flows down with the local velocity to the next cross flow plane, where the second new born vortex will apear. In this way the computation proceeds on successively from section to section.

With proper selection of the time step Δt and the number of vorticity piece N_W including the new born leading edge vorticity piece, we can have N_W equations to satisfy N_W boundary conditions including eq.(3) and Kutta condition eq.(4). They are:

$$[C_{ij}][\gamma_j]=-[V_{ni}] \quad , \quad \begin{matrix} i=1,2,\cdots N_W \\ j=1,2,\cdots N_W \end{matrix} \qquad (5)$$

where $[C_{ij}]$ is the matrix of influence coefficients, γ_j is the strength of the jth vortex piece, V_{ni} is the normal induced velocity at the ith control point that can be determined by the known γ_j at the former section. Thus the γ_j can be determined for the considered cross flow plane by solving the eq.(5). As the computation proceeds forwards, the roll-up of the separated vortices along x-axis and the pressure loads exerting on the wing can be determined.